EXTRACELLULAR AND SARCOMERIC ALTERATIONS IN MARFAN SYNDROME: INSIGHTS FROM AORTIC FIBRILLIN-1 AND MYOCARDIAL TITIN INVESTIGATIONS

PhD Thesis (short version)

Cristina-Maria Șulea, MD

Semmelweis University Doctoral School
Cardiovascular Medicine and Research Division

Supervisors: Miklós Kellermayer, MD, DSc
Zoltán Szabolcs, MD, PhD

Official reviewers: Zoltán Péter Jakus, MD, PhD
Attila Borbély, MD, PhD

Head of the Complex Examination Committee:
Zoltán Benyó, MD, DSc

Members of the Complex Examination Committee:
Bálint Dér, MD, PhD
Márton Kolossváry, MD, PhD

Budapest
2025

1. Introduction

Marfan syndrome (MFS) is the most prevalent and extensively studied fibrillinopathy, with an estimated prevalence of 1 in 5,000 individuals worldwide. It results from pathogenic variants in the fibrillin-1 gene (*FBN1*), which occur *de novo* in approximately 25% of cases but are more commonly inherited in an autosomal dominant pattern. The resulting molecular dysfunction typically involves either a dominant-negative (DN) effect, where a full complement of fibrillin-1 molecules is synthesised but the mutant monomers are structurally impaired; or haploinsufficiency (HI), resulting in a quantitative deficiency of functional fibrillin-1 due to loss of one functional allele.

At the tissue level, fibrillin-1 molecules assemble into microfibrils – beaded extracellular matrix (ECM) structures with integral mechanical and signaling roles. A key function of these microfibrils is the sequestration of transforming growth factor-β (TGF-β), the dysregulation of which is considered central to MFS pathogenesis. The widespread expression of fibrillin-1 underlies the multisystemic nature of MFS, with cardiovascular manifestations, particularly aortic disease, representing the major source of morbidity and mortality. Increasing evidence also supports the existence of primary left

ventricular (LV) impairment, raising the concept of an intrinsic "Marfan cardiomyopathy".

Cardiomyopathies are a heterogeneous group of disorders marked by structural and functional myocardial impairment, with dilated cardiomyopathy (DCM) being the most common form. Around 40% of DCM cases are linked to truncating variants in the gene encoding the protein titin (*TTN*tv), a major determinant of passive myocardial tension. Titin functions as a molecular spring within the half-sarcomere and exists in two main cardiac isoforms: the shorter, stiffer N2B and the longer, more compliant N2BA. Their relative expression reflects species-specific hemodynamic demands, with an N2BA:N2B ratio of around 0.5 in healthy human myocardium and approximately 1 in DCM.

While TGF-β dysregulation is considered central to MFS pathophysiology, direct nanoscale studies of human aortic fibrillin-1 microfibril architecture remain lacking. However, biochemical disruption and structural/mechanical failure may act synergistically, with impaired microfibrils contributing to or exacerbating tissue dysfunction. Moreover, the partial phenotypic overlap between MFS-associated myocardial changes and DCM warrants investigation of potentially shared molecular pathways.

2. Objectives

This work aimed to provide novel insights into the molecular impact of MFS on the cardiovascular system by:

1. investigating the morphological and nanomechanical properties of individual fibrillin-1 microfibrils isolated from human aortic tissue in MFS and non-MFS individuals. This included:

a. assessing structural dimensions and stiffness of human aortic fibrillin-1 microfibrils using AFM;

b. evaluating the impact of *FBN1* mutations on the morphology and biomechanics of single fibrillin-1 microfibrils in MFS;

c. exploring potential associations between types of *FBN1* mutations and measured biophysical parameters, thereby contributing to improved genotype-phenotype correlations.

2. exploring the possible role of sarcomeric titin in the myocardial impairment observed in Marfan cardiomyopathy by analyzing total titin levels and titin isoform expression in LV myocardial tissue from MFS patients using molecular biology techniques.

3. Methods

The studies were designed and conducted in accordance with the Declaration of Helsinki (1975, revised 2013) and was approved by the Medical Research Council of Hungary (TUKEB 73/2005, ETT TUKEB 7891/2012/EKU (119/PI/12.), ETT TUKEB 12751-3/2017/EKU, ETT TUKEB IV/10161-1/2020/EKU, and ETT TUKEB BM/17671-3/2024). Written informed consent was obtained from all participants prior to inclusion. All surgical procedures were performed at the Heart and Vascular Center of Semmelweis University. The experimental work was carried out at the Department of Biophysics and Radiation Biology of Semmelweis University.

3.1. Fibrillin-1 study

The cohort included 10 genetically confirmed MFS patients (MFS group, MFS1–MFS10) undergoing aortic root reconstruction for MFS-related complications, segregated by *FBN1* mutation effect into DN (n = 5) and HI (n = 5) subgroups. For comparison, non-MFS aortic tissue was obtained from 10 control individuals (control group, C1–C10) undergoing heart transplantation for ischemic cardiomyopathy.

3.1.1. Fibrillin-1 microfibril purification

Following the removal of adventitial tissue, a full-thickness aortic wall piece weighing roughly 1 gram was

minced, homogenized in 5 mL of 0.05 M Tris-HCl buffer (0.4 M NaCl, 0.01 M CaCl2, 0.01% NaN3, 10 mM NEM, 2 mM PMSF, pH 7.4), and digested with type 1A bacterial collagenase for 4 hours at room temperature. Digestion was stopped by adding 100 µL EDTA, and the homogenate was centrifuged at 10,000 g for 30 minutes. The supernatant ("low-salt extract") was filtered and stored at 4°C. The pellet was re-extracted in 5 mL of 0.05 M Tris-HCl buffer (1 M NaCl, 10 mM EDTA, 0.01% NaN3, 10 mM NEM, 2 mM PMSF, pH 7.4) for 48 hours at 4°C, followed by centrifugation and filtration ("high-salt extract"). Both extracts were subjected to size-exclusion chromatography on a Sepharose CL-2B column in 0.05 M Tris-HCl buffer (0.4 M NaCl, 0.01% NaN3, pH 7.4) and 1 mL fractions corresponding to chromatogram peaks were collected. Protein content was quantified by measuring ultraviolet light absorbance (280 nm), and high-protein fractions were selected for atomic force microscopy (AFM) imaging.

3.1.2. AFM imaging

AFM is a high-resolution technique used to visualize and probe materials at the nanoscale. A sharp tip mounted on a cantilever scans the sample surface, and cantilever deflections, detected via a laser and photodetector, are converted into three-dimensional topographical maps with (sub)nanometer

resolution. In tapping mode, the tip oscillates above the surface, minimizing damage to soft biological specimens. AFM can also perform force spectroscopy to measure local mechanical properties, including stiffness (Young's modulus). Its ability to operate in air or aqueous environments allows the investigation of hydrated, dynamic systems under near-physiological conditions with minimal sample preparation or fixation.

3.1.2.1. Morphological measurements

20 µL of suspension were deposited onto freshly cleaved mica, allowed to equilibrate for 15 minutes, rinsed with ultrapure water, and dried under nitrogen gas stream. Topographical images were recorded in tapping mode using an Asylum Research Cypher ES microscope (Oxford Instruments) with OMCL-AC160TS-R3 microcantilevers (Olympus Corporation; 26 N/m, 300 ± 100 kHz) at a setpoint of 700 mV and 512 × 512-pixel resolution. Images were analyzed using Igor Pro 6 (WaveMetrics) and Gwyddion.

The morphological analysis of individual fibrillin-1 microfibrils focused on the bead regions, including their maximum and average height, length, width, projected area, volume, roundness, and aspect ratio, but concerned also interbead height, periodicity, and microfibril length.

Comparison analyses were performed between the MFS and control groups, with additional subgroup comparisons to assess genotype-specific effects.

3.1.2.2. Mechanical investigation

Force spectroscopy was performed in liquid at room temperature. Poly-L-lysine-coated mica substrates were incubated with 100 µL of sample for 15 minutes, then washed and covered with 1.5 mL buffer. Microfibril bead stiffness was measured using a DriveAFM instrument (Nanosurf AG) equipped with BL-AC40TS cantilevers (Olympus Corporation; 0.1 N/m, 110 ± 35 kHz), calibrated by the thermal method. Force mapping was conducted at a 500 pN setpoint, and Young's modulus values were determined by fitting the Hertzian model to the approach segment of the recorded force-distance curves, assuming a conical indenter geometry and Poisson's ratio of 0.25. Height and modulus maps were processed in Gwyddion.

3.2. Titin study

Human LV septal myocardial samples were obtained from 12 MFS patients (labeled PAP). Myocardial tissue from two *TTN*tv- DCM patients and one adult male Wistar rat (HK9) served as controls and reference specimens. Previously investigated *TTN*tv- DCM samples were used for comparison.

3.2.1. Protein solubilization and titin isoform analysis

The LV myocardial fragments (10–15 mg) were homogenized in glass Dounce tissue grinders under liquid nitrogen, incubated at -20°C for 20 minutes, and solubilized at 60°C for 15 minutes in 50% urea buffer (8 M urea, 2 M thiourea, 50 mM Tris-HCl, 75 mM DTT, 3% SDS, 0.03% bromophenol blue, pH 6.8) mixed with 50% glycerol and protease inhibitors (0.04 mM E64, 0.16 mM leupeptin, 0.2 mM PMSF). Solubilized samples were centrifuged at 16,000 g for 5 minutes, aliquoted, snap-frozen, and stored at -80 °C.

Titin expression was analyzed by 1% SDS-agarose gel electrophoresis (16 mA/gel, 3.5 h), followed by overnight SYPRO Ruby staining (Thermo Fischer Scientific) and imaging with a Typhoon laser scanner (Amersham Biosciences). Band optical densities were quantified using ImageJ (NIH) to calculate the N2BA:N2B isoform ratio. Full-length titin (T1), its degradation product (T2), and total titin (TT) were normalized to the myosin heavy chain (MHC).

3.2.2. Titin truncated protein detection

Western blotting was used to verify whether additional gel bands represented truncated titin fragments. Samples were separated on 0.8% SDS-agarose gels, transferred to PVDF membranes (Amersham Biosciences), and incubated overnight

at 4°C with anti-T12 (N-terminal; University of Bonn, Germany; 1:1,000) and anti-M8M10 (C-terminal; Myomedix, GmbH; 1:1,000) primary antibodies, followed by CyDye-conjugated secondary antibodies (Amersham Biosciences). Blots were imaged with a Typhoon scanner (Amersham Biosciences), and band intensities were quantified in ImageJ (NIH), with truncated titin normalized to full-length T1.

3.3. Statistical analysis

Statistical analyses were performed in GraphPad Prism 8 (GraphPad Software). Outliers were identified and excluded using the ROUT method (Q = 1%). For pooled analyses, all original data points were included, and outliers were reassessed. Normality was evaluated using the Shapiro-Wilk or Anderson-Darling test, depending on dataset size. Data are presented as mean ± SD or median (Q1–Q3). Two-group comparisons employed unpaired Student's t-test with Welch's correction for unequal variances or the Mann-Whitney U test, while categorical variables were analyzed with Fisher's exact test. For comparisons among more than two groups, the Kruskal-Wallis test with Dunn's post hoc correction was applied. Correlations were assessed using Pearson or Spearman tests as appropriate, with regression lines plotted to illustrate relationships. Significance was defined as $P < 0.05$.

4. Results

4.1. Fibrillin-1 study

4.1.1. Morphological assessment

AFM imaging revealed fibrillin-1 microfibrils with preserved morphology across all samples (**Figure 1**), displaying the characteristic "beads-on-a-string" appearance with globular beads connected by filamentous interbead regions. For analysis, only relatively linear, non-entangled segments were selected, yielding 4,370 beads from 176 microfibrils (MFS: 98 microfibrils, 2,229 beads; controls: 78 microfibrils, 2,141 beads). **Figure 2** summarizes the comparative analysis of fibrillin-1 microfibril morphology between each genetic subgroup and controls.

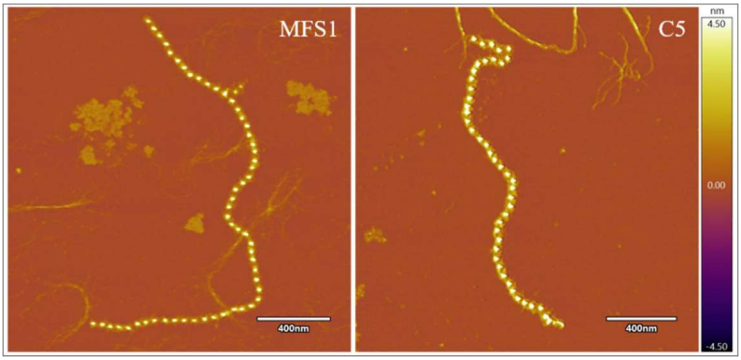

Figure 1. AFM imaging of fibrillin-1 microfibrils isolated from MFS and control aorta.

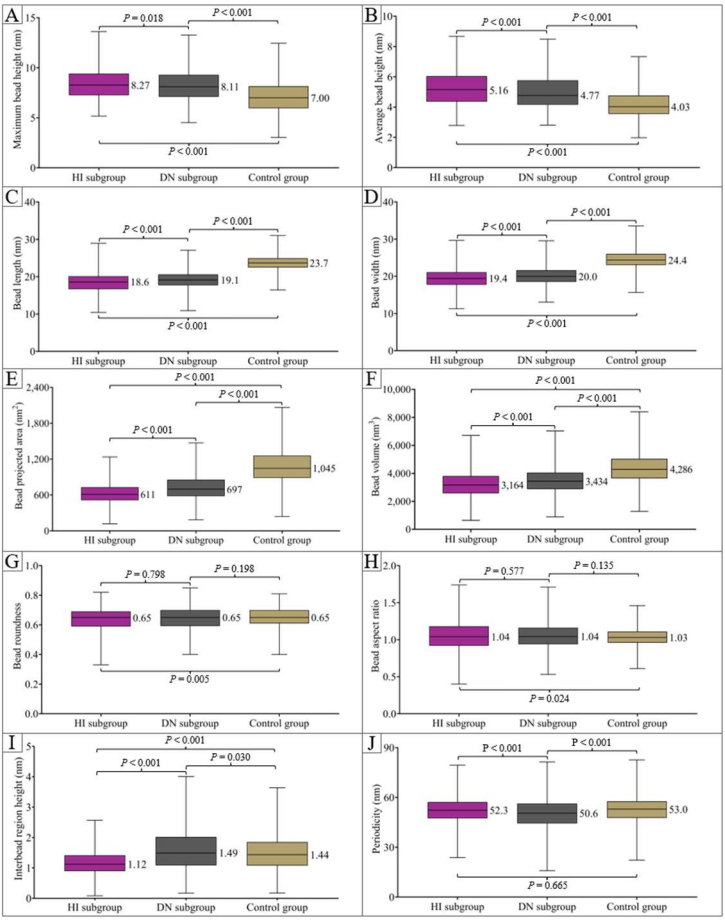

Figure 2. Comparison of fibrillin-1 microfibril morphological parameters in MFS samples and controls: maximum (**A**) and average (**B**) bead height, length (**C**), width (**D**), projected area (**E**), volume (**F**), roundness (**G**), and aspect ratio (**H**), interbead region height (**I**), and periodicity (**J**).

Purified microfibril length reached up to 15 µm, most measuring around 0.5–2 µm (**Figure 3**). Analysis of 1,010 fibrillin-1 microfibrils showed no significant length differences between MFS and controls or between HI and DN subgroups.

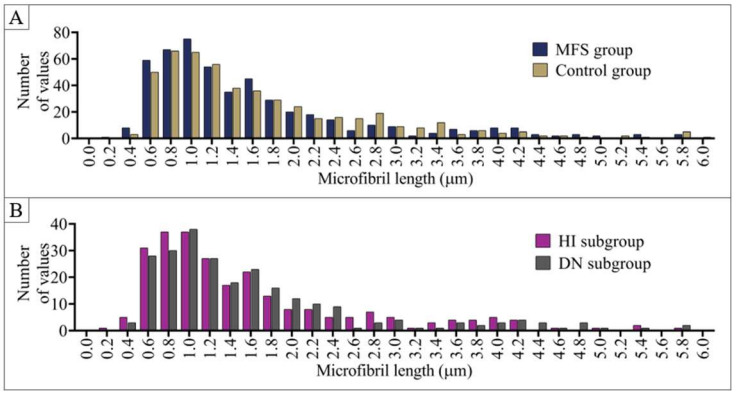

Figure 3. Fibrillin-1 microfibril length distribution within the MFS and control groups (**A**), and across the HI and DN subgroups (**B**).

4.1.2. Mechanical investigation

In force-mapping AFM, 3,930 beads from 281 microfibrils were analyzed. MFS samples showed greater variability and an overall lower median Young's modulus than controls. The HI subgroup exhibited significantly lower stiffness than both DN and control groups ($P < 0.001$), whereas DN and control samples did not differ significantly ($P = 0.327$) (**Figure 4**).

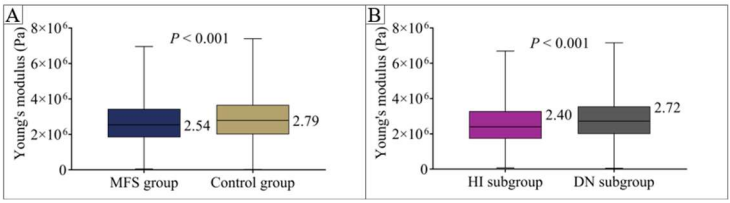

Figure 4. Young's modulus comparison between MFS and control groups (**A**), and between HI and DN subgroups (**B**).

Force spectroscopy revealed possible indentation-like events on a subset of approach curves (100–130 per sample), interpreted as indicative of disruptive tip-sample interactions. The median indentation force was lower in MFS than controls (178 [IQR 107–262] vs. 240 [170–340] pN, P < 0.001). HI and DN subgroups showed similar forces (182 [116–258] vs. 177 [102–265] pN, P = 0.322), both significantly lower than controls (P < 0.001) (**Figure 5**).

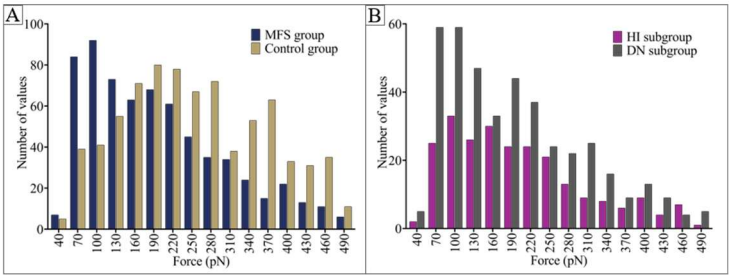

Figure 5. Indentation peak analysis from AFM force-distance curves, comparing the distribution of force values between the MFS and control cohorts (**A**), and between the HI and DN subgroups (**B**).

4.2. Titin study

4.2.1. Proteomic analysis

SDS-agarose gel electrophoresis showed clear N2BA and N2B titin isoform bands in PAP and DCM samples, with the rat control predominantly expressing N2B. Several PAP samples (notably PAP100 and PAP104) displayed additional bands above MHC (**Figure 6**).

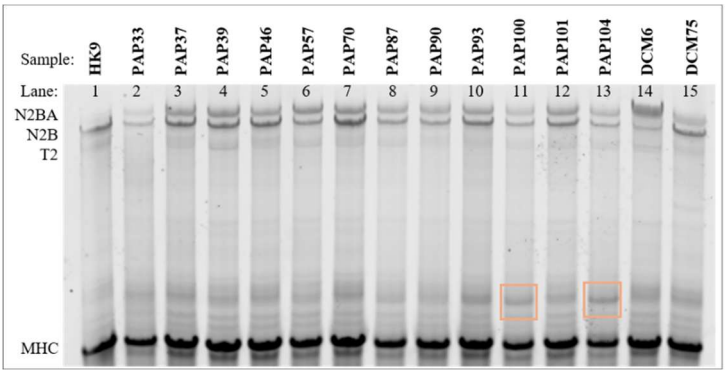

Figure 6. 1% SDS-agarose gel analysis of included samples. The beige squares highlight the observed additional bands.

TT levels (T1 + T2) were 0.19 ± 0.03, comparable to normal human myocardium (0.20–0.23) and included *TTN*tv-DCM samples (0.19 ± 0.05), while T1 expression was significantly lower in PAP than in *TTN*tv- DCM samples (0.15 ± 0.03 vs. 0.22 ± 0.08, $P < 0.001$). Densitometry revealed a mean N2BA:N2B ratio of 0.71 ± 0.19, higher than in the

control rat heart (0.28) and healthy donor hearts (approximately 0.4–0.56), yet lower than in *TTN*tv- DCM specimens (0.84 ± 0.19, P = 0.045) (**Table 1**). Western blotting showed weak T12 labeling and no M8M10 signal in the additional bands, suggesting N-terminal titin fragments related to T2.

Table 1. Proteomic analysis of titin isoforms in PAP samples.

Sample ID	N2BA:N2B	T1:MHC	T2:MHC	TT:MHC
PAP33	0.41	0.08	0.05	0.13
PAP37	0.67	0.18	0.05	0.23
PAP39	0.70	0.17	0.05	0.22
PAP46	0.53	0.16	0.05	0.21
PAP57	1.08	0.15	0.04	0.19
PAP70	0.49	0.19	0.04	0.24
PAP87	0.80	0.15	0.04	0.19
PAP90	0.87	0.12	0.03	0.16
PAP93	0.62	0.15	0.05	0.20
PAP100	0.72	0.11	0.04	0.15
PAP101	0.78	0.16	0.05	0.21
PAP104	0.86	0.14	0.06	0.20
Mean	0.71	0.15	0.05	0.19
SD	0.19	0.03	0.01	0.03

These findings indicate preserved TT levels but reduced T1 content and a marked shift toward the more compliant N2BA isoform in MFS hearts, mirroring patterns observed in DCM and suggesting potential molecular mechanisms underlying Marfan cardiomyopathy.

4.2.2. Clinical correlations

Potential correlations between the N2BA:N2B ratio and clinical or echocardiographic parameters were examined (**Figure 7**). Three patients (PAP33, PAP90, PAP100) exhibited LV enlargement, but given the small cohort size and generally preserved cardiac function, no clear associations could be observed.

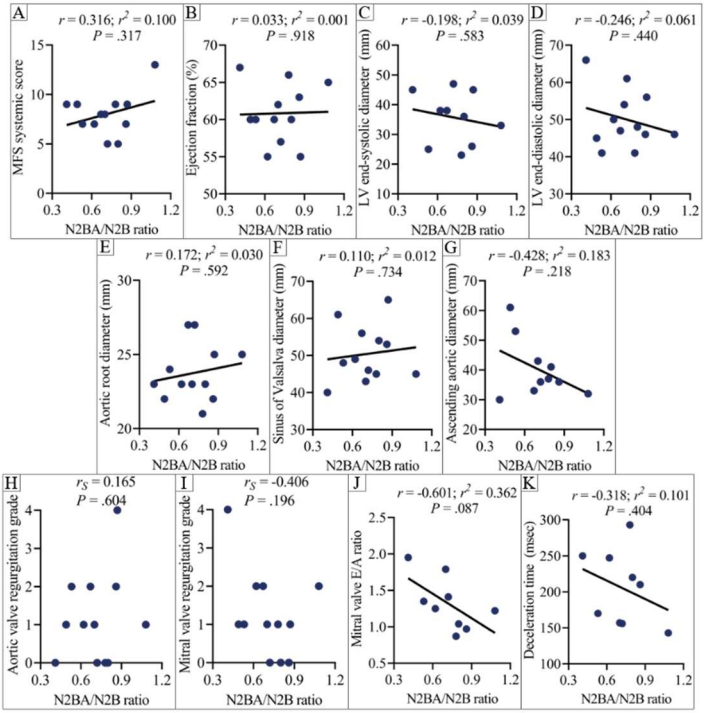

Figure 7. Correlation analyses between the N2BA:N2B ratio in PAP samples and selected clinical and echocardiographic parameters.

5. Conclusions

1. Our analysis provided a detailed characterization of human aortic fibrillin-1 microfibrils. AFM imaging revealed pronounced morphological alterations in MFS microfibrils, including reduced bead and interbead dimensions, suggestive of disturbed molecular organization. Force spectroscopy demonstrated significantly reduced transverse stiffness, most notably in samples harboring haploinsufficient *FBN1* variants, and revealed failure-like events at the bead level, indicating a compromised ability of MFS microfibrils to withstand mechanical stress.

2. Proteomic profiling of LV myocardium showed a shift in titin isoform composition toward the more compliant N2BA isoform, without changes in total titin content, likely representing an adaptive response aimed at mitigating the increased passive myocardial stiffness under conditions of ECM dysfunction in the context of MFS.

These findings provide molecular and biomechanical evidence that *FBN1* mutations compromise microfibril integrity in the aortic wall and lead to myocardial titin remodeling. Both mechanisms may contribute to the vascular fragility and intrinsic myocardial dysfunction characteristic of MFS.

6. Bibliography of the candidate's publications

6.1. Articles related to the PhD thesis (Σ IF = 7.8)

Șulea CM, Mártonfalvi Z, Csányi C, Haluszka D, Pólos M, Ágg B, Stengl R, Benke K, Szabolcs Z, Kellermayer MSZ. Nanoscale Structural Comparison of Fibrillin-1 Microfibrils Isolated from Marfan and Non-Marfan Syndrome Human Aorta. Int J Mol Sci. 2023;24(8):7561. **IF: 4.9**

Kellermayer D, **Șulea CM***, Tordai H, Benke K, Pólos M, Ágg B, Stengl R, Csonka M, Radovits T, Merkely B, Szabolcs Z, Kellermayer M, Kiss B. Marfan syndrome cardiomyocytes show excess of titin isoform N2BA and extended sarcomeric M-band. J Gen Physiol. 2025;157(3):e202413690. *: shared first authorship. **IF: 2.9**

6.2. Other articles (Σ IF = 17.418)

Pólos M, **Șulea CM**, Benke K, Ágg B, Kovács A, Hartyánszky I, Merkely B, Schäfers HJ, Szabolcs Z. Giant unruptured sinus of Valsalva aneurysm successfully managed with valve-sparing procedure - a case report. J Cardiothorac Surg. 2020;15(1):6. **IF: 1.637**

Pólos M, Domokos D, **Şulea CM**, Benke K, Csikós G, Nagy A, Skoda R, Szabó A, Merkel E, Hartyánszky I, Szabolcs Z, Merkely B, Becker D. Needle in the heart: a rare case of cardiac tamponade caused by a migrated foreign body and mimicking ST segment elevation myocardial infarction. BMC Cardiovasc Disord. 2021;21(1):143. **IF: 2.174**

Pólos M, Stengl R, **Șulea CM**, Benke K, Bartha E, Ágg B, Koppányi Á, Hartyánszky I, Székely A, Németh E, Kovács A, Merkely B, Szabolcs Z. Stratégiai szemléletváltás a Marfan-szindrómás betegeken végzett aortagyök-rekonstrukciókban [Changing strategies in aortic root reconstruction in Marfan syndrome]. Orv Hetil. 2021;162(18):696–704. **IF: 0.707**

Șulea CM*, Lakatos B, Kovács A, Benke K, Suhai FI, Csulak E, Merkel E, Nagy B, Hartyánszky I, Merkely B, Szabolcs Z, Pólos M. Blood-filled cyst of the tricuspid valve: Multiple cardiac disorders, one surgical case. J Card Surg. 2022;37(1):245–248. *: shared first authorship. **IF: 1.6**

Șulea CM, Nădășan V, Ursachi T, Toboltoc PC, Benedek T. What Patients Find on the Internet When Looking for Information About Percutaneous Coronary Intervention: Multilanguage Cross-sectional Assessment. J Med Internet Res. 2022;24(12):e41219. **IF: 7.4**

Șulea CM, Csobay-Novák C, Oláh Z, Banga P, Szeberin Z, Soltész Á, Jokkel Z, Benke K, Csonka M, Merkel ED, Merkely B, Szabolcs Z, Pólos M. Staged Hybrid Repair of a Complex Type B Aortic Dissection. J Cardiovasc Dev Dis. 2022;9(9):297. **IF: 2.4**

Șulea CM*, Kiss AB, Ágg B, Benke K, Bartha E, Szilveszter B, Stengl R, Csonka M, Szabolcs Z, Pólos M. Pregnancy-related chronic type A aortic dissection highlights the importance of thorough prenatal maternal examination. J Cardiothorac Surg. 2025;20(1):105. *: shared first authorship. **IF: 1.5**